

# Robust Impedance Control of Robots Using an Adaptive Interaction Force Observer

Yanjun WANG<sup>1,2</sup>, Yunfei ZHANG<sup>1,2</sup>, Shujun GAO<sup>1,2</sup>, Clarence W. DE SILVA<sup>2</sup>

(1.ViWiSTAR Technologies Ltd., Vancouver, Canada, V6T 1Z4;

2.Dept. of Mechanical Engineering, The University of British Columbia, Vancouver, Canada, V6T 1Z4)

**Abstract:** For robot interaction control, the interaction force between the robot and the manipulated object or environment should be monitored. Impedance control is a type of interaction control. Specifically, in impedance control, the dynamic relationship between the interaction force and the resulting motion is controlled. In order to control the impedance of a mechanical system, typically, the interaction force has to be sensed. Due to the inherent limitations of direct force sensing at the interaction site, in the present work, the interaction force is observed using robust observers. In particular, to enhance the accuracy of impedance control, a first order sliding mode impedance controller is designed and incorporated in the present paper. Its advantage over position-based interaction control algorithms is demonstrated through experimentation. Experimental results are given to show the effectiveness of the proposed algorithms.

**Key words:** Interaction Control, Impedance Control, Neural Networks, Sliding Mode Observer, Sliding Mode Control.

## 1 Introduction

Besides motion control of a robot manipulator, the control of the dynamic interaction when the manipulator is constrained by the interacting objects is also an important problem in practice. Several algorithms of interaction control have been proposed by researchers in the past<sup>[1-3]</sup>. Depending on whether there is an explicit closed loop with respect to the force tracking error, interaction control algorithms can be classified into indirect interaction control schemes and direct interaction force control schemes. In hybrid force/motion control, the workspace is decomposed into force controlled directions and motion controlled directions<sup>[4]</sup>. However, in practice, this decomposition is difficult<sup>[5]</sup>. Impedance control as an interaction control methodology was applied in several past studies since the seminal work of Hogan<sup>[6]</sup>. The objective of impedance control is to control the dynamic relationship between the robot end-effector motion and the interaction force during interaction. It is termed an indirect force control methodology since neither the motion nor the interaction

force is explicitly controlled. It has been proved to be effective, particularly because it tends to mimic manipulation by human hand, and has been used in engineering applications such as parts assembly<sup>[7-8]</sup>.

The interaction force provides the most direct information about the state of mechanical interaction. In impedance control implementations, the interaction force information is required to shape the impedance function in the desired manner. However, accurate interaction force information is not readily available in practical applications. Usually, to sense the interaction force between a robot manipulator and an interacted object, a force sensor is mounted in the wrist. The sensed interaction force information has to be calibrated and filtered before it is applied in the impedance controller since the sensed interaction force is an internal force at the robotic wrist rather than the real interaction force between the robot manipulator end-effector and the interacted environment<sup>[9-10]</sup>. As pointed out<sup>[11-13]</sup>, the application of a force sensor may introduce some unavoidable problems, such as sensing noise, limited bandwidth,

self-varying properties due to temperature change, and the difficulty of proper location of the force sensor at the interaction site. Reconstructing the interaction force by the use of estimation algorithms is preferable for these reasons, and has been widely used<sup>[11, 13-14]</sup>. Much of such work assumed an accurate dynamic model of the robot manipulator. Offline identification algorithms for robot dynamics may be used to identify the dynamic parameters. However, the resulting accuracy is not satisfactory due to the fact that the friction component in each joint is non-linear and uncertain<sup>[21-22]</sup>.

As noted, the velocity information is required in impedance control algorithms. Unfortunately, in the robot manipulator under study, only a joint position encoder is provided in each joint. The velocity information that is obtained by differentiation is typically noisy and unacceptable in experimental implementations<sup>[25-28]</sup>. Simultaneous estimation of joint velocity and external force is desirable. Recently, sliding mode observer, which is a robust observation algorithm, had found application in this field. A second-order sliding mode observers was applied to estimate both velocity and external interaction force<sup>[29-31]</sup>. The estimated values were applied in a sliding, mode-based impedance controller to guarantee realization of the desired impedance. Experimental results were given to show the effectiveness of the algorithm. In that work, however, the external interaction force estimation was obtained after passing through a low-pass filter. The filter presents a tradeoff between the smoothness and the time lag of the reconstructed interaction force.

The present work is inspired by the early work presented in<sup>[32-38]</sup>. However, the present approach can provide a more accurate interaction force estimation while generating a velocity estimation as well, which is required in impedance control algorithms. Robust impedance shaping algorithms are designed in the present paper using the reconstructed interaction force. The structure of the rest of the paper is as follows. In Section 2, the robot dynamic model is ex-

pressed and identified. Simultaneous velocity and external force estimation are proposed in Section 3, using an adaptive high order sliding mode observer. In Section 4, the robust impedance controller is developed, which uses the estimated velocity and the external interaction force. In Section 5 the advantage of the proposed impedance control algorithm is demonstrated by experimentally comparing it with other interaction control algorithms. Concluding remarks are given in the final section.

## 2 Problem Formulation

The platform that is used in the present work is a commercial four-degree-of-freedom robot manipulator called Whole Arm Manipulator (WAM), as shown in Fig. 1. The first and the third joints are fixed in order to simplify it as a planar two-link manipulator.

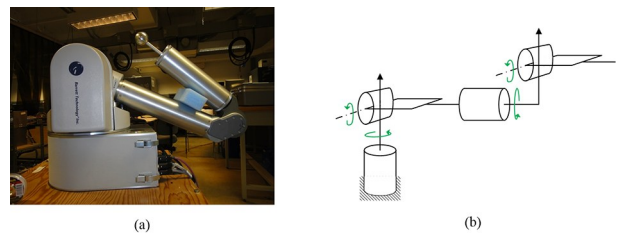


Fig. 1 (a) WAM; (b) Schematic representation of WAM.

The schematic representation of the simplified two-link manipulator is given in Fig. 2.

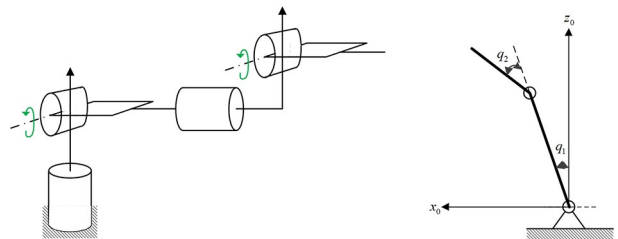


Fig. 2 Schematic representation and coordinate frame of the simplified two-link WAM.

The robot manipulator is equipped with joint position encoders only. Unfortunately, there are no force sensor and a joint tachometer, to sense the interaction force and the joint velocity. Hence, observers are designed in the present work to estimate the

interaction force and the joint velocity, simultaneously. It is found through validation experiments that the manufacturer-provided dynamic parameters are not accurate<sup>[33]</sup>.

### 3 Interaction Force Estimation

The joint space dynamic model of the robot manipulator is given by

$$M(q)\ddot{q} + C(q, \dot{q})\dot{q} + F_v\ddot{q} + F_c \text{sgn}(\dot{q}) + G(q) = \tau - J^T(q)F_e \quad (1)$$

where,

$q$ -joint position vector (2×1)

$\dot{q}$ -joint velocity vector (2×1)

$\ddot{q}$ -joint acceleration vector (2×1)

$M(q)$ -inertia matrix (2×2)

$C(q, \dot{q})$ -Coriolis and Centrifugal matrix (2×2)

$F_v$ -viscous friction matrix (2×2)

$F_c$ -Coulomb friction matrix (diagonal 2×2)

$\text{sgn}(\dot{q})$ -2×1 vector whose components are sign functions of the joint velocity

$G(q)$ -gravity vector (2×1)

$\tau$ -joint actuator torque vector (2×1)

$J(q)$ -Jacobian of the manipulator (2×2)

$F_e$ -external interaction force vector (2×1)

In order to enhance the accuracy of interaction force estimation, the dynamic parameters of the manipulator are identified through experimental data. An offline dynamic parameter identification algorithm could be used to obtain the dynamic parameters. However, due to the uncertainty of the friction parameter in each joint, the identified model could not accurately characterize the dynamics of the manipulator.

A neural network with one hidden layer and the back propagation algorithm is used in the present work for parameter identification. Since the joint torque residue calculation is based on the states of two joints, the compensation torques for joint 1 and joint 2 are considered simultaneously using one neural network, as shown in Fig.3.

Eight hidden layer nodes are used. Also,  $w_{ij}$  = connection weight between the input layer and the hidden layer;  $w_{jk}$  = connection weight between the

hidden layer and the output layer;  $\Delta\tau_1$  = torque compensation for joint 1; and  $\Delta\tau_2$  = torque compensation for joint 2.

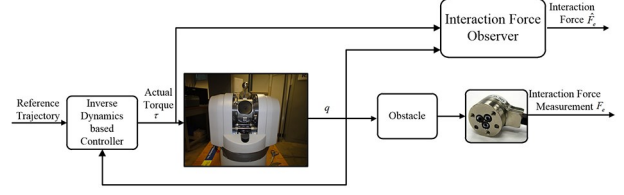


Fig. 3 The validation scheme of the interaction force estimation.

The sigmoid function is used as the activation unction, as given by

$$\sigma(x) = \frac{1}{1+e^{-x}} \quad (2)$$

The input to the neural network is the joint motion state, which is given by the corresponding joint position  $q$  and velocity  $\dot{q}$ . The joint acceleration  $\ddot{q}$  is provided as well. The velocity and acceleration information are reconstructed using the sliding mode-based robust differentiator. The output of the neural network is the torque difference between the actual joint torques calculated using the joint actuator current and the predicted joint torques. The neural network is trained using the inputs and the corresponding outputs. After training, it will act as a compensator to compensate for the torque difference that will be used in the interaction force estimation algorithms. The offline identified dynamic parameters together with the neural network-based compensator are able to predict the joint torque accurately, as shown in Fig. 4 and Fig. 5.

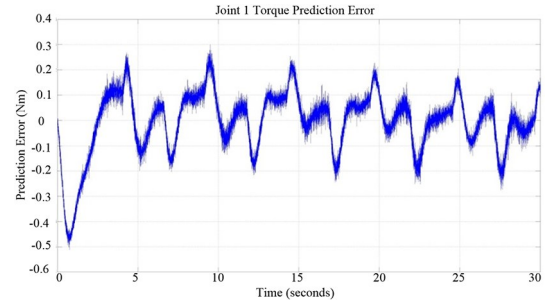


Fig. 4 Joint 1 torque prediction error.

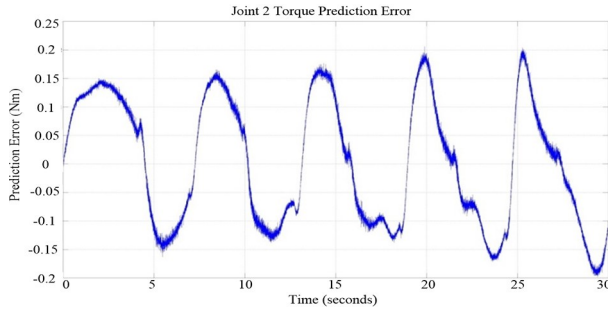


Fig. 5 Joint 2 torque prediction error.

An interaction force estimation algorithm that uses an adaptive high order sliding mode observer is proposed in this section. It provides robust interaction force estimation in the presence of measurement noise. The dynamic model of the robot manipulator as given in Eq. (1) is rewritten in the state-space form now. Let  $x_1 = q$ ,  $\dot{x}_1 = \dot{q}$ , and  $u = \tau$ . Then, the joint space robot dynamic equation may be represented in the state-space form as,

$$\begin{aligned} \dot{x}_1 &= x_2; \\ \dot{x}_2 &= f(t, x_1, x_2, u) + \xi(t, x_1, x_2, u) \end{aligned} \quad (3)$$

$y = x_1$   
where,

$$f(t, x_1, x_2, u) = -M^{-1}(x_1) [C(x_1, x_2)x_2 + F_v x_2 + F_c \text{sgn}(x_2) + G(x_1) - u]$$

$$\xi(t, x_1, x_2, u) = -M^{-1}(x_1) [\Delta\tau + J^T(X_1)F_e];$$

$x_1 \in R^2$  is the joint position encoder reading;  $x_2 \in R^2$  is the joint velocity vector of the manipulator;  $f(t, x_1, x_2, u) \in R^2$  represents the nominal dynamics of the mechanical system; and  $\xi(t, x_1, x_2, u)$  is the combination of the model error-induced terms  $\Delta\tau$  (reconstructed from the neural network-based compensator) and the external interaction force  $F_e$ . The representations of  $f(t, x_1, x_2, u) \in R^2$  and  $\xi(t, x_1, x_2, u)$  are given by

$$f(t, x_1, x_2, u) = \begin{bmatrix} f_1(t, x_1, x_2, u) \\ f_2(t, x_1, x_2, u) \end{bmatrix} \quad (4)$$

$$\xi(t, x_1, x_2, u) = \begin{bmatrix} \xi_1(t, x_1, x_2, u) \\ \xi_2(t, x_1, x_2, u) \end{bmatrix} \quad (5)$$

The non-adaptive high order sliding mode observer has been implemented<sup>[30]</sup> to reconstruct the external disturbance. The limitation of this algorithm

is that it is extremely difficult to determine the observer gains to guarantee the convergence of the observer. Adaptive sliding mode-based differentiators have been proposed<sup>[34-35]</sup>. The observer gains could be tuned on line to guarantee the convergence of the robust differentiator.

Inspired by the work in [34-35], an adaptive sliding mode observer is designed here to reconstruct the interaction force. It is given by Eq. (6)-Eq. (8). The observer adaption laws are designed based on the Lyapunov method, as presented by

$$\begin{aligned} \dot{\hat{x}}_{1i} &= \hat{x}_{2i} + \hat{\lambda}_{2i} |x_{1i} - \hat{x}_{1i}|^{2/3} \text{sign}(x_{1i} - \hat{x}_{1i}) \\ &+ k_{2i}(x_{1i} - \hat{x}_{1i}) \end{aligned} \quad (6)$$

$$\begin{aligned} \dot{\hat{x}}_{2i} &= f_i(x_1, \hat{x}_2, u) + \hat{\lambda}_{1i} |\dot{x}_{1i} - \hat{x}_{2i}|^{1/2} \text{sign}(\dot{x}_{1i} - \hat{x}_{2i}) + \\ &k_{1i}(\dot{x}_{1i} - \hat{x}_{2i}) + \dot{z}_i \end{aligned} \quad (7)$$

$$\dot{\hat{z}}_{1i} = \hat{\lambda}_{0i} \text{sign}(\dot{x}_{1i} - \hat{x}_{2i}) \quad (8)$$

where  $\hat{\lambda}_{2i}$ ,  $\hat{\lambda}_{1i}$  and  $\hat{\lambda}_{0i}$  are gains to be determined to guarantee the convergence of the estimation error.

For the derivation simplicity, a matrix representation is used for the observer described by the following equations:

$$\dot{\hat{x}}_1 = \hat{x}_2 + \hat{\lambda}_2 |x_1 - \hat{x}_1|^{2/3} \text{sign}(x_1 - \hat{x}_1) + k_2(x_1 - \hat{x}_1) \quad (9)$$

$$\begin{aligned} \dot{\hat{x}}_2 &= f(x_1, \hat{x}_2, u) + \hat{\lambda}_1 |\dot{x}_1 - \hat{x}_2|^{1/2} \text{sign}(\dot{x}_1 - \hat{x}_2) + k_1 \\ &(\dot{x}_1 - \hat{x}_2) + \dot{z} \end{aligned} \quad (10)$$

$$\dot{\hat{z}} = \hat{\lambda}_0 \text{sign}(\dot{x}_1 - \hat{x}_2) \quad (11)$$

The variables in Eq. (9) -Eq. (11) are in fact vector representations of the scalars in Eq. (6) -Eq. (8). The adaption laws are given as

$$\dot{\hat{\lambda}}_2 = s_2 |s_2|^{2/3} \text{sign}(s_2) \quad (12)$$

$$\dot{\hat{\lambda}}_1 = s_1 |s_1|^{1/2} \text{sign}(s_1) \quad (13)$$

$$\dot{\hat{\lambda}}_0 = s_1 \int_0^t \text{sign}(s_1) dt \quad (14)$$

$$s_2 = x_1 - \hat{x}_1 \quad (15)$$

$$s_1 = \dot{x}_1 - \hat{x}_2 \quad (16)$$

The proof of convergence of this sliding mode observer is given in terms of the homogeneity of differential inclusions and the Lyapunov approach. After convergence, it is able to accurately reconstruct

the interaction force as well as the velocity information. The results of the interaction force reconstruction for two directions are given in Fig. 6 and Fig. 7.

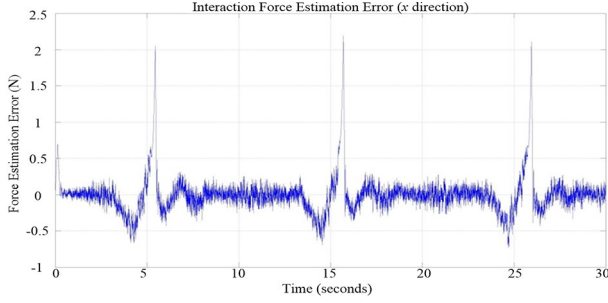


Fig. 6 Force estimation error (x direction).

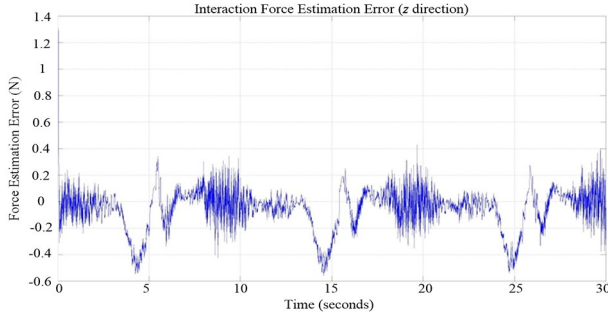


Fig. 7 Force estimation error (z direction).

## 4 Robust Impedance Control

Robust impedance controllers are designed in this section. The interaction force reconstructed by the observer is used in impedance shaping. To show the advantage of the robust impedance controller that is designed here, impedance control accuracy is defined. Sliding mode-based impedance controller is formulated after that.

### 4.1 Cartesian Space Trajectory Selection

To show the effectiveness of impedance control as an interaction control algorithm, a common Cartesian space trajectory is planned for the end-effector to follow. The end-effector will interact with the obstacle by following this trajectory. The derivatives of this reference trajectory are directly used in the control algorithms. Hence, it is desirable to have smooth reference trajectories for both velocity and acceleration.

In the reference trajectory selection, the specific

application should also be considered. In the present project of robotic homecare, the robot end-effector is commanded to follow a reference trajectory to come in contact with the human body. The initial Cartesian space position of the robot end-effector is  $(-0.04691, 0.1193)$ . The interacted object is located at  $(0.08, 0.6)$  in the Cartesian space. After reaching the object, the end-effector is made to exert some periodic motion on the object.

Taking all the factors discussed above into consideration, the reference trajectories are divided into two phases. The switching between the two phases happens at  $t=2.0$  sec. In the first phase, the end-effector in the Cartesian space is commanded to move to some adjacent region of the designated position. When the end-effector is in the designated location, it is commanded to execute a desired periodical motion. Since there are six known conditions (initial position, initial velocity, initial acceleration, final position, final velocity, and final acceleration) in phase 1, a fifth-order polynomial is used to describe the trajectory in this phase.

For the x direction, with  $x(0) = -0.4691$ ,  $\dot{x}(0) = 0$ ,  $\ddot{x}(0) = 0$ ,  $x(2) = 0.1$ ,  $\dot{x}(2) = 0$ ,  $\ddot{x}(2) = 0$  the reference trajectory determined as

$$x(t) = 0.1067 \cdot t^5 - 0.5335 \cdot t^4 + 0.7114 \cdot t^3 - 0.4691, \quad t \in [0, 2] \quad (17)$$

Similarly, the reference trajectory for the z direction is determined as

$$z(t) = 0.0651 \cdot t^5 - 0.3381 \cdot t^4 + 0.4759 \cdot t^3 - 1.193, \quad t \in [0, 2] \quad (18)$$

After determining the phase 1 polynomial trajectory, the velocity and acceleration at  $t=2$  sec are known as well.

There are three known conditions for phase 2. A sinusoidal waveform is used to describe the periodic motion in both directions. However, there should be four known conditions in order to completely describe a sinusoidal signal. One can assign any of these four to a specified value, in order to have a closed form solution. In the z direction, it is reasonable to set the amplitude of the sinusoidal wave as

0.1. For the x direction, the position is assumed to be the constant location 0.1.

Then, the sinusoidal waveforms for the x and z directions, when  $t \in [2.0, 10]$ , are determined as

$$x(t) = 0.1 \quad (19)$$

$$z(t) = 0.1 \sin(1.272t - 1.8780) + 0.5382 \quad (20)$$

The designed Cartesian space trajectories are shown in Fig. 8. The corresponding joint space position trajectories are shown in Fig. 9. It is seen from the joint space reference trajectories that the position of joint 2 will never become 0 or  $\pi$ , which means the manipulator will not be in the singularity configurations if the trajectory tracking performance is good.

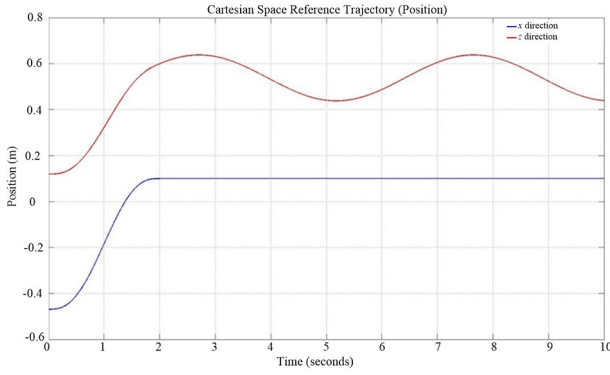


**Fig. 8 Cartesian space reference trajectories (for interaction control).**

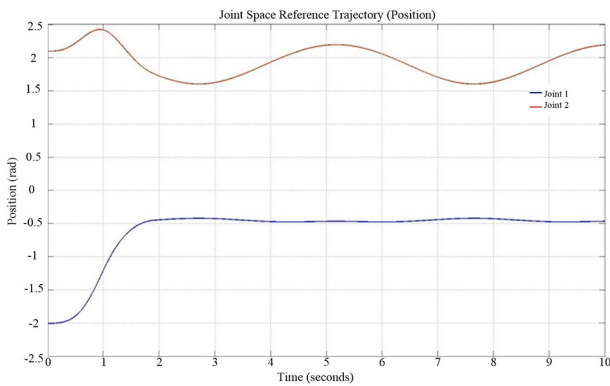


**Fig. 9 Joint space reference trajectories (for interaction control).**

## 4.2 Impedance Control Accuracy

The accuracy of impedance control corresponds to the extent to which the ideal impedance model is

realized. This is discussed here, particularly to compare the performance of different impedance control algorithms that are proposed. The desired impedance model is described by

$$M_d(\ddot{X} - \ddot{X}_d) + B_d(\dot{X} - \dot{X}_d) + K_d(X - X_d) = \hat{F}_e \quad (21)$$

where

$M_d$ -desired inertia matrix ( $2 \times 2$ )

$B_d$ -desired damping matrix ( $2 \times 2$ )

$K_d$ -desired stiffness matrix ( $2 \times 2$ )

$X$ -Cartesian space actual position vector ( $2 \times 1$ )

$X_d$ -Cartesian space desired position vector ( $2 \times 1$ )

$\hat{F}_e$ -estimated external interaction force vector ( $2 \times 1$ )

$\hat{F}_e$ -estimated external interaction force vector ( $2 \times 1$ )

Let  $\tilde{X} = X - X_d$ . Then Eq. (21) can be rewritten as

$$M_d \ddot{\tilde{X}} + B_d \dot{\tilde{X}} + K_d \tilde{X} - \hat{F}_e = 0 \quad (22)$$

Define the following matrix variable:

$$I_e = M_d \ddot{\tilde{X}} + B_d \dot{\tilde{X}} + K_d \tilde{X} - \hat{F}_e \quad (23)$$

If  $I_e = \text{diag}(0, 0)$ , then the desired impedance is realized.

It is noticed that the estimated interaction forces have some residue with respect to the measured ones. This is unavoidable no matter what type of system identification algorithm is used to identify the dynamic model of the manipulator.

## 4.3 Robust Impedance Control

A sliding surface is defined as

$$s = \int_0^t M_d^{-1} \cdot \dot{I}(\tau) d\tau \quad (24)$$

The finite-time convergent adaptive high-order sliding mode observer that has been proposed in Section 4 is used here for the estimation of the external interaction force and velocity. Since the observed states are used, the matrix variable in Eq. (23) is redefined as

$$\hat{I}_e = M_d(\hat{X}_2 - \ddot{X}_d) + B_d(\hat{X} - \dot{X}_d) + K_d(\hat{X} - X_d) = \hat{F}_e \quad (25)$$

where,

$\hat{X}_2$ -Cartesian space estimated velocity vector ( $2 \times 1$ )

$\hat{X}_1$ -Cartesian space estimated position vector ( $2 \times 1$ )

$\dot{\hat{X}}_2$ -Cartesian space estimated acceleration vector (2×1)

They may be obtained from the adaptive high-order sliding mode observer as proposed in Section 4, using the forward kinematic relationship. Also, these variables may be directly reconstructed from the Cartesian space version of this adaptive high order sliding mode observer.

The sliding surface should be a function of the system states. In the state-space representation of the robot manipulator, the state variables should be position and velocity. The acceleration is not a state in the state-space representation. The sliding variable is represented in the integral form given by

$$s = \begin{bmatrix} s_1 \\ s_2 \end{bmatrix} = \int_0^t M_d^{-1} \cdot \hat{I}(\tau) d\tau = 0 \quad (26)$$

The derivative of this sliding surface is given as

$$\dot{s} = M_d^{-1} \cdot \hat{I}(\tau) = \dot{\hat{X}} - \ddot{X} + M_d^{-1} B_d (\hat{X}_2 - \dot{X}_d) + M_d^{-1} K_d (\hat{X}_1 - X_d) - M_d^{-1} \hat{F}_{ee} \quad (27)$$

Substituting the equation for the external interaction force observer into Eq. (27), we have

$$\dot{s} = M_c^{-1}(X_1) F_\tau - M_c^{-1}(X_1) H(X_1, \hat{X}_2) + \lambda_1 |\dot{\hat{X}}_1 - \dot{\hat{X}}_2|^{1/2} \cdot \text{sign}(\dot{\hat{X}}_1 - \dot{\hat{X}}_2) + K_1(X_1 - \hat{X}_1) + \dot{Z} - \ddot{X}_d + M_d^{-1} B_d (\hat{X}_2 - \dot{X}_d) + M_d^{-1} K_d (\hat{X}_1 - X_d) - M_d^{-1} \hat{F}_{ee} \quad (28)$$

The control law, which drives the system states onto this manifold, is given by

$$F_\tau = H(X_1, \hat{X}_2) - M_c(X_1) \lambda_1 |\dot{\hat{X}}_1 - \dot{\hat{X}}_2|^{1/2} \cdot \text{sign}(\dot{\hat{X}}_1 - \dot{\hat{X}}_2) - M_c(X_1) K_1 (X_1 - \hat{X}_1) - M_c(X_1) \dot{Z} + M_c(X_1) \ddot{X}_d - M_c(X_1) M_d^{-1} B_d (\hat{X}_2 - \dot{X}_d) - M_c(X_1) M_d^{-1} K_d (\hat{X}_1 - X_d) + M_c(X_1) M_d^{-1} \hat{F}_{ee} - M_c(X_1) \cdot K_g \cdot \text{sign}(s) \quad (29)$$

$$K_g = \begin{bmatrix} k_{g1} \\ k_{g2} \end{bmatrix} \quad (30)$$

where,  $k_{g1} > 0$ ,  $k_{g2} > 0$  are parameters to be tuned to guarantee the stabilizing feature of this controller.

This control law will lead to the following representation of  $\dot{s}$ :

$$\dot{s} = -K_g \cdot \text{sign}(s) \quad (31)$$

Define

$$k_{\min} = \min(k_{g1}, k_{g2}) \quad (32)$$

The finite time convergence of this controller may be proved by using the Lyapunov function given by

$$V = \frac{1}{2} s^T s = \frac{1}{2} \|s\|_2^2 \quad (33)$$

Taking the time derivative of  $V$  along the trajectories of the system, we have

$$\begin{aligned} \dot{V} &= s^T \dot{s} = -s^T \cdot K_g \cdot \text{sign}(s) = \\ &= -k_{g1} s_1 \cdot \text{sign}(s_1) - k_{g2} s_2 \cdot \text{sign}(s_2) = \\ &= -k_{g1} |s_1| - k_{g2} |s_2| \leq \\ &= -k_{\min} (|s_1| + |s_2|) = -k_{\min} \|s\|_1 \end{aligned} \quad (34)$$

In view of the real vector norms given in Eq. (35), and using them in the derivatives of the Lyapunov function, we have Eq. (36) for the derivative of the Lyapunov function:

$$\|s\|_2 \leq \|s\|_1 \quad (35)$$

$$\dot{V} \leq -k_{\min} \|s\|_1 \leq -k_{\min} \|s\|_2 \quad (36)$$

Eq. (36) can be further simplified as

$$\dot{V} \leq -\sqrt{2} k_{\min} V^{1/2} \quad (37)$$

The stability of the plant under the proposed impedance controller is easy to verify. The finite-time convergence is further proved here, which is an important feature of the proposed controller.

Integrating both sides of Eq. (37) over the time interval  $[0, t]$  we get

$$V^{1/2}(t) \leq -\sqrt{2} k_{\min} t + V^{1/2}(0) \quad (38)$$

Thus,  $V(t)$  reaches zero in finite time  $T_r$  bounded by

$$T_r \leq \frac{-\sqrt{2} V^{1/2}(0)}{k_{\min}} \quad (39)$$

Note that a faster convergence can be realized by increasing the value of  $k_{\min}$ . However, the side-effect of this increase is the increased magnitude of the discontinuous term in the control input described by Eq. (30). Chattering in this case will become more problematic. This results in a tradeoff between the convergence rate and the side-effect of chattering. The impedance control results are shown in Fig.10-Fig.11.

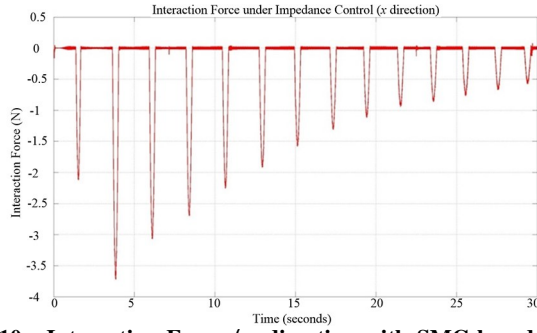


**Fig. 10** Interaction Force (*x* direction with SMC-based impedance control algorithms).

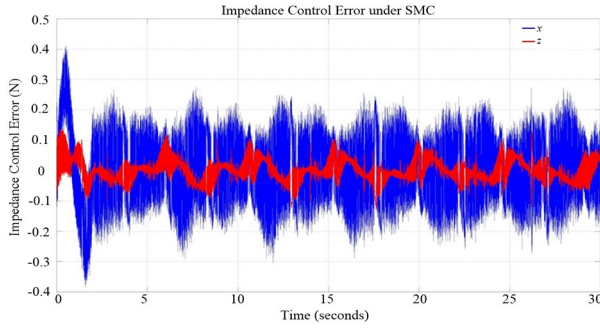


**Fig. 11** Impedance control accuracy (with SMC-based impedance control algorithms).

## 5 Comparison with Other Interaction Control Algorithms

Two other interaction control algorithms are given in this section and are compared with the robust impedance controller as proposed in Section 4.

### 5.1 Inverse Dynamics-based Impedance Control

According to the Cartesian space dynamic model and the desired impedance model, the torque command to be sent to the joint actuator is given by

$$\begin{aligned} \tau = & [J^T(q) + M(q)J(q)^{-1}M_d^{-1}] \hat{F}_e + C(q, \dot{q})\dot{q} + \\ & F_c \cdot \text{sign}(\dot{q}) + F_v \cdot \dot{q} + G(q) + M(q)J(q)^{-1}\ddot{X}_d - \\ & M(q)J(q)^{-1}[M_d^{-1}B_d(J(q)\dot{q} - \dot{X}_d) + M_d^{-1}K_d \\ & (X(q) - \dot{X}_d)] + M(q)J(q)^{-1}\dot{J}(q)\dot{q} \end{aligned} \quad (40)$$

where,  $X(q)$  is the Cartesian space position of the manipulator end-effector, as calculated by the forward kinematics equation. Joint space adaptive high-order sliding mode observer is used here to simultaneously estimate the joint velocity and the interaction force.

The impedance control results are given in Fig. 12-Fig. 13. When compared with the sliding mode-based impedance controller, it is observed that the impedance control accuracy is worse. In the initial phase, the impedance control error is large. Sliding mode-based impedance controller is able to limit the impedance control error within a small range.

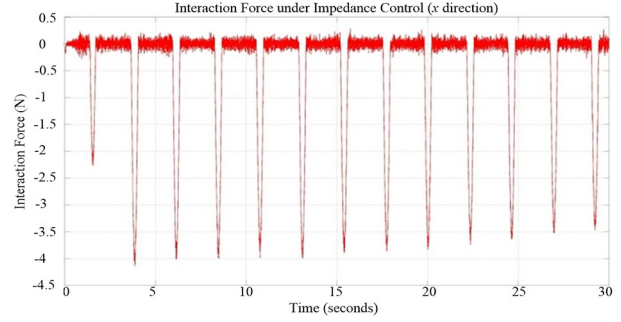


**Fig. 12** Interaction Force (*x* direction with inverse dynamics-based impedance control algorithms).

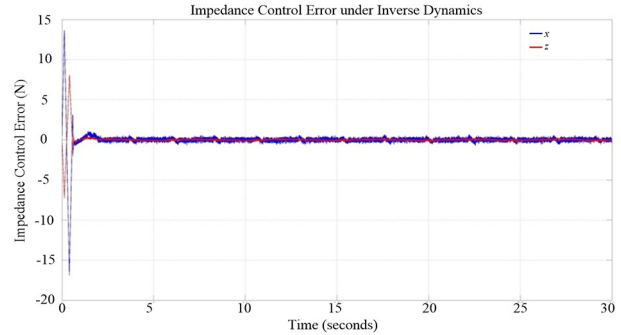


**Fig. 13** Impedance control accuracy (with inverse dynamics-based impedance control algorithms).

### 5.2 Interaction Control through Position Control

Interaction force can be controlled through exclusive position control approaches. Then, the interaction force is taken as a disturbance. The position control system calculates the desired actuator torque so that the reference trajectory is tracked. It may generate excessive interaction force during interaction, which has to be avoided.

If the interaction force has to be modulated, the mechanical properties of the environment have to be accurately known. However, the mechanical properties of the environment are difficult to obtain. It is

shown that an excessive interaction force may be present when pure position control strategies are used in interaction control. This will serve as the control group to show the advantage of impedance control when it is used as the interaction control strategy.

The Cartesian space inverse dynamics-based trajectory tracking controller is used here. This control algorithm is given by

$$\begin{aligned} \tau = & M(q)J^{-1}(\dot{q})[-\dot{J}(\dot{q})\dot{q} + \ddot{X}_d K_D(\dot{X}_d - \dot{X}) + K_p \\ & (X_d - X)] + C(q, \dot{q})\dot{q} + F_c \cdot \text{sign}(\dot{q}) + F_v \cdot \dot{q} + \\ & G(q) + J^T(q)\hat{F}_e \end{aligned} \quad (41)$$

After simplification, the trajectory tracking problem can be described by

$$\ddot{X} - \ddot{X}_d + K_D(\dot{X} - \dot{X}_d) + K_p(X - X_d) = 0 \quad (42)$$

Here  $K_p$  and  $K_D$  are the corresponding proportional and derivative gains. It is seen that in this case, the interaction control problem is transformed into a pure trajectory tracking scheme, which means the controller renders the manipulator infinitely stiff. Then, the external interaction force is considered as the external disturbance to be rejected by the trajectory tracking algorithm. It is observed from Fig. 14 that the interaction force is increasing, and the system appears unstable. It follows that interaction control through pure position control is not practical.

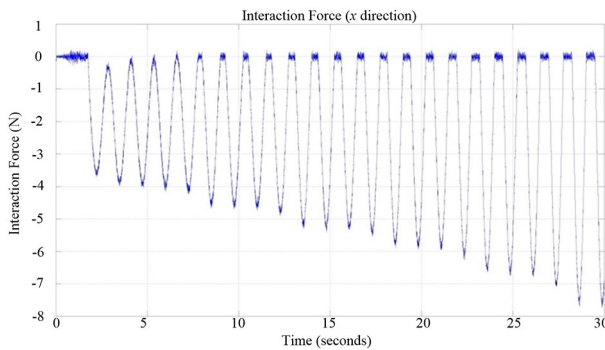


**Fig. 14 Interaction force under pure position control (x direction).**

## 6 Conclusion

Impedance control is an indirect force control algorithm. In this paper it was used as an approach

of interaction control. Interaction force and velocity of the manipulator are required in impedance control. However, force sensor has inherent limitations, which make its use in interaction control somewhat impractical. For these reasons, an adaptive high-order sliding mode observer was proposed to simultaneously estimate the external interaction force and velocity. The estimated interaction force and velocity were used in the impedance control algorithms. A sliding mode impedance controller was proposed to shape the impedance of the robot manipulator. This impedance controller was shown to outperform the conventional inverse dynamics-based impedance controller in terms of the impedance control accuracy. Also, impedance control was compared with pure position control-based interaction control to show the advantage of the former.

## References

- [ 1 ] Whitney, D. E. (1987). Historical perspective and state of the art in robot force control. *The International Journal of Robotics Research*, pp.3-14.
- [ 2 ] Zeng, G. and Hemami, A. (1997). An overview of robot force control. *Robotica*, pp.473-482.
- [ 3 ] Garcia, G. J., Corrales, J. A., Pomares, J. and Torres, F. (2009). Survey of visual and force/tactile control of robots for physical interaction in Spain. *Sensors*, pp.9689-9733.
- [ 4 ] Raibert, M.H. and Craig, J.J. (1981). Hybrid position/force control of manipulators. *Journal of Dynamic Systems, Measurement, and Control*, pp.126-133.
- [ 5 ] De Schutter, J., Bruyninckx, H., Zhu, W.H. and Spong, M.W. (1998). Force control: A bird's eye view. In *Control Problems in Robotics and Automation*, pp. 1-17.
- [ 6 ] Hogan N. (1984). "Impedance control: an approach to manipulation," *Proceedings of American Control Conference*, San Diego, CA, Jun., pp. 304-313.
- [ 7 ] Hogan N. (1984) "Impedance control of industrial robots," *Robot Computing and Integrated Manufacturing*, pp. 99-113.
- [ 8 ] Hogan, N. (1989). May. Controlling impedance at the man/machine interface. In *IEEE. Proceedings, 1989 International Conference on Robotics and Auto-*

- tion, pp. 1626-1631.
- [ 9 ] García, J.G., Robertsson, A., Ortega, J.G. and Johansson, R. (2008). Sensor fusion for compliant robot motion control. *IEEE Transactions on Robotics*, pp.430-441.
- [10] Kato, A. and Ohnishi, K. (2006). Robust force sensorless control in motion control system. In *9th IEEE International Workshop on Advanced Motion Control*, 2006, IEEE. pp. 165-170.
- [11] Murakami, T., Nakamura, R., Yu, F. and Ohnishi, K. (1993). Force sensorless impedance control by disturbance observer. In *Conference Record of the Power Conversion Conference-Yokohama*, IEEE. pp. 352-357.
- [12] Mitsantisuk, C., Ohishi, K. and Katsura, S. (2011). Estimation of action/reaction forces for the bilateral control using Kalman filter. *IEEE Transactions on Industrial Electronics*, pp.4383-4393.
- [13] Khalil, I.S. and Sabanovic, A. (2010). Sensorless action-reaction-based residual vibration suppression for multi-degree-of-freedom flexible systems. In *IECON 2010-36<sup>th</sup> Annual Conference on IEEE Industrial Electronics Society*, IEEE. pp. 1633-1638.
- [14] Khalil, I.S. and Sabanovic, A. (2011). Sensorless torque/force control. *Advances in Motor Torque Control*, pp.49-69.
- [15] Jeong, J.W., Chang, P.H. and Park, K.B. (2011). Sensorless and modeless estimation of external force using time delay estimation: application to impedance control. *Journal of Mechanical Science and Technology*, p.2051.
- [16] Son, H.I., Bhattacharjee, T. and Lee, D.Y. (2010). Estimation of environmental force for the haptic interface of robotic surgery. *The International Journal of Medical Robotics and Computer Assisted Surgery*, pp. 221-230.
- [17] Van Damme, M., Beyl, P., Vanderborght, B., Grosu, V., Van Ham, R., Vanderniepen, I., Matthys, A. and Lefeber, D. (2011). Estimating robot end-effector force from noisy actuator torque measurements. In *2011 IEEE International Conference on Robotics and Automation*, IEEE, pp. 1108-1113.
- [18] Katsura, S., Matsumoto, Y. and Ohnishi, K. (2007). Modeling of force sensing and validation of disturbance observer for force control. *IEEE Transactions on Industrial Electronics*, pp.530-538.
- [19] Murakami, T., Yu, F. and Ohnishi, K. (1993). Torque sensorless control in multidegree-of-freedom manipulator. *IEEE Transactions on Industrial Electronics*, pp.259-265.
- [20] Gupta, A. and O' Malley, M.K. (2011). Disturbance-observer-based force estimation for haptic feedback. *Journal of Dynamic Systems, Measurement, and Control*, p.014505.
- [21] Bona, B. and Indri, M. (2005). Friction compensation in robotics: an overview. In *Proceedings of the 44th IEEE Conference on Decision and Control*, IEEE, pp. 4360-4367.
- [22] Van Geffen, V. (2009). A study of friction models and friction compensation. *DCT*, 118, p.24.
- [23] Marban, A., Srinivasan, V., Samek, W., Fernández, J. and Casals, A. (2018). October. Estimation of interaction forces in robotic surgery using a semi-supervised deep neural network model. In *2018 IEEE/RSJ International Conference on Intelligent Robots and Systems (IROS)*, IEEE. pp. 761-768.
- [24] Popov, D. and Klimchik, A. (2019). March. Real-Time External Contact Force Estimation and Localization for Collaborative Robot. In *2019 IEEE International Conference on Mechatronics (ICM)*, IEEE. pp. 646-651.
- [25] Yih, C.C. (2012). *Extended Nicosia-Tomei velocity observer-based robot-tracking control*. *IET Control Theory & Applications*, pp.51-61.
- [26] Lotfi, N. and Namvar, M. (2010). *A globally convergent observer for velocity estimation in robotic manipulators with uncertain dynamics*. In *2010 IEEE International Conference on Robotics and Automation*, IEEE pp. 4645-4650.
- [27] Daly, J.M. and Wang, D.W. (2009). *Bilateral teleoperation using unknown input observers for force estimation*. In *2009 American Control Conference*, IEEE. pp. 89-95.
- [28] Daly, J.M. and Wang, D.W. (2009). *Output feedback sliding mode control in the presence of unknown disturbances*. *Systems & Control Letters*, pp.188-193.
- [29] Daly, J.M. and Wang, D.W. (2013). *Time-delayed output feedback bilateral teleoperation with force estimation for n-DOF nonlinear manipulators*. *IEEE Transactions on Control Systems Technology*, pp. 299-306.
- [30] Van, M., Kang, H.J. and Suh, Y.S. (2013). *Second*

order sliding mode-based output feedback tracking control for uncertain robot manipulators. *International Journal of Advanced Robotic Systems*, p.16.

- [31] Park, J.H. and Cho, H.C. (1999). *Sliding-mode controller for bilateral teleoperation with varying time delay*. In 1999 IEEE/ASME International Conference on Advanced Intelligent Mechatronics, *IEEE*. pp. 311-316.
- [32] Sidhom, L., Pham, M.T., Thévenoux, F. and Gautier, M. (2010). *Identification of a robot manipulator based on an adaptive higher order sliding modes differentiator*. In 2010 IEEE/ASME International Conference on Advanced Intelligent Mechatronics, *IEEE*. pp. 1093-1098.
- [33] Wang, Y. and de Silva, C.W. (2014). *An experimental setup for dynamics control of robot manipulators*. In 2014 9th International Conference on Computer Science & Education, *IEEE*. pp. 123-128.
- [34] Sidhom, L., Smaoui, M., Thomasset, D., Brun, X. and Bideaux, E. (2011). *Adaptive higher order sliding modes for two-dimensional derivative estimation*. *IFAC Proceedings Volumes*, pp.3063-3071.
- [35] Yuan, Y., Wang, Y. and Guo, L. (2018). *Force reflecting control for bilateral teleoperation system under time-varying delays*. *IEEE Transactions on Industrial Informatics*, pp.1162-1172.
- [36] Su, H., Yang, C., Ferrigno, G., & De Momi, E. (2019). *Improved human-robot collaborative control of redundant robot for teleoperated minimally invasive surgery*. *IEEE Robotics and Automation Letters*, pp. 1447-1453.
- [37] Dong, K., Liu, H., Zhu, X., Wang, X., Xu, F., & Liang, B. (2019). *Force-free control for the flexible-joint robot in human-robot interaction*. *Computers & Electrical Engineering*, pp. 9-22.
- [38] Sundaralingam, B., Lambert, A. S., Handa, A., Boots, B., Hermans, T., Birchfield, S., ... & Fox, D. (2019, May). *Robust learning of tactile force estimation through robot interaction*. In 2019 IEEE International Conference on Robotics and Automation (ICRA), pp. 9035-9042.

## Authors' Biographies



**Yanjun WANG**, obtained his PhD degree in the Department of Mechanical Engineering, The University of British Columbia, Vancouver, Canada in 2014. He received his Master's degree in Automotive Engineering from Shanghai Jiao Tong University, Shanghai, China in 2009, and his Bachelor's degree in Automotive Engineering from Nanjing University of Aeronautics & Astronautics, Nanjing, Jiangsu, China in 2006. Presently he works on compliance control of robotics in ViWiSTAR Technologies Ltd.. His research interests are in robot dynamics modeling and control, system identification, automotive powertrain system modeling, control and optimization, and soft computing. Email: yjwang@alumni.ubc.ca.



**Yunfei ZHANG**, received his B.S. degree in automation from Qingdao University of Science and Technology in 2006, and M.S. degree in automotive engineering from Shanghai Jiao Tong University, China, in 2010. He finished his Ph.D. degree in the Department of Mechanical Engineering at the University of British Columbia, Canada in 2015. He currently works on robotics technologies for caring elderly people, as an ambitious start up entrepreneur. His main research interests include deep reinforcement learning and control, decision making, robotics, and autonomous driving. Email: yunfeizhang0616@gmail.com



**Shujun GAO**, received his B.S. degree from North University of China in 2008, and M.S. degree from Tianjin University, China, in 2010. He finished his Ph.D. degree in the Department of Mechanical Engineering at the University of British Columbia, Canada in 2017. His main research interests include deep learning, computer vision, and engineering optimization. Email: shujun.gao@mech.ubc.ca



**Clarence W. de Silva**, received Ph.D. degrees from Massachusetts Institute of Technology, Cambridge, MA, in 1978, and the University of Cambridge, Cambridge, U. K., in 1998, the Honorary D.Eng. degree from the University of Waterloo, Waterloo, ON, Canada, in 2008, and the higher doctorate, Sc. D., from the University of Cambridge, in 2020.

He is a Professor of Mechanical Engineering at the University of British Columbia, Vancouver, BC, Canada, since 1988. His appointments include the Tier 1 Canada Research Chair in Mechatronics and Industrial Automation, Professorial Fellow, Peter Wall Scholar, Mobil Endowed Chair Professor, and NSERCBC Packers Chair in Industrial Automation. He has authored 25 books and about 560 papers, approximately

half of which are in journals. His recent books, published by Taylor & Francis/CRC Press, include *Modeling of Dynamic Systems-With Engineering Applications* (2018), *Sensor Systems* (2017), *Sensors and Actuators-Engineering System Instrumentation*, 2nd Edition (2016), *Mechanics of Materials* (2014), *Mechatronics-A Foundation Course* (2010), *Modeling and Control of Engineering Systems* (2009), and *VIBRATION-Fundamentals and Practice*, 2nd Edition (2007); and by Addison Wesley, *Soft Computing and Intelligent Systems Design-Theory, Tools, and Applications* (with F. Kararay, 2004).

Prof. de Silva is a Fellow of the American Society of Mechanical Engineers (ASME), the Institution of Electrical and Electronics Engineers (IEEE), the Canadian Academy of Engineering, and the Royal Society of Canada.

Email:desilva@mech.ubc.ca



**Copyright:** © 2019 by the authors. This article is licensed under a Creative Commons Attribution 4.0 International License (CC BY) license (<https://creativecommons.org/licenses/by/4.0/>).